

Synthetic Routes for the Preparation of Silver Nanoparticles

A Mechanistic Perspective

Natalia L. Pacioni, Claudio D. Borsarelli, Valentina Rey and Alicia V. Veglia

Abstract In this chapter, we revise some of the most relevant and widely used synthetic routes available for the preparation of metallic silver nanoparticles. Particular emphasis has been focused in the rationale involved in the formation of the nanostructures, from the early metallic silver atoms formation, passing by atoms nucleation and concluding in the growth of silver nanostructures. We hope the reader will find in this chapter a valuable tool to better understand the relevance of the experimental conditions in the resulting silver nanoparticle size, shape and overall properties.

1 Introduction

Silver nanoparticles (AgNP) are already part of our daily life, being present in clothes (e.g. in socks); household and personal care products, mainly due to their antimicrobial properties [1, 2], see Chaps. “[Biomedical Uses of Silver Nanoparticles: From Roman Wine Cups to Biomedical Devices](#)” and “[Anti-microbiological and Antiinfective Activities of Silver](#)”.

Furthermore, as discussed in the previous chapter, their unique physical and electronic properties make them excellent candidates for different applications e.g. Surface Enhanced Raman Spectroscopy (SERS) [3–9]. The optical properties of AgNP depend

N.L. Pacioni (✉) · A.V. Veglia

INFIQC, CONICET and Departamento de Química Orgánica-Facultad de Ciencias
Químicas-Universidad Nacional de Córdoba, Ciudad Universitaria, Edificio Ciencias II,
Haya de la Torre y Medina Allende s/n, X5000HUA Córdoba, Argentina
e-mail: nataliap@fcq.unc.edu.ar

C.D. Borsarelli (✉) · V. Rey

Laboratorio de Cinética y Fotoquímica (LACIFO), Centro de Investigaciones
y Transferencia de Santiago del Estero (CITSE-CONICET), Universidad Nacional de
Santiago del Estero (UNSE), RN9, Km 1125. Villa El Zanjón,
CP 4206 Santiago del Estero, Argentina
e-mail: cdborsarelli@gmail.com

on characteristics such as size, shape and capping-coating. Synthetic approaches for the preparation of AgNP continue to grow as evidenced from the quasi-exponential increase in the number of articles published over the last two decades (Fig. 1).

Generally, the methods used for the preparation of metal nanoparticles can be grouped into two different categories *Top-down* or *Bottom-up*. Breaking a wall down into its components—the bricks, represents the *Top-down* approach, Fig. 2. While building up “the brick” from clay-bearing soil, sand, lime and water would represent *Bottom-up*, Fig. 2. Thus, in nanosciences *Top-down* involves the use of bulk materials and reduce them into nanoparticles by way of physical, chemical or mechanical processes whereas *Bottom-up* requires starting from molecules or atoms to obtain nanoparticles [10].

Top-down fabrication of nanomaterials usually comprise mechanical-energy, high energy lasers, thermal and lithographic methods. Examples of these categories include, but are not limited to, Atomization, Annealing, Arc discharge, Laser ablation, Electron beam evaporation, Radio Frequency (RF) sputtering and Focused ion beam lithography [10].

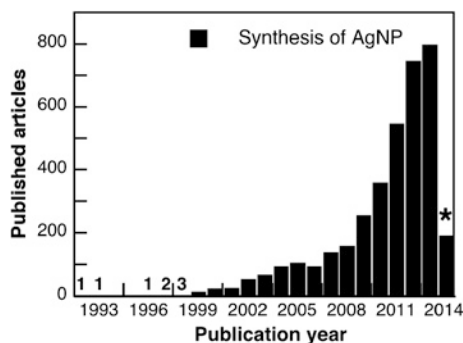


Fig. 1 Representation of the number of research articles published in the period 1992–2014 according to Scopus® containing the term “synthesis of silver nanoparticles” as keyword. Inset numbers indicate (from left to right) the amount of articles published in 1992, 1993, 1996, 1997 and 1998. The asterisk indicates that this result is partial (January–April 2014)

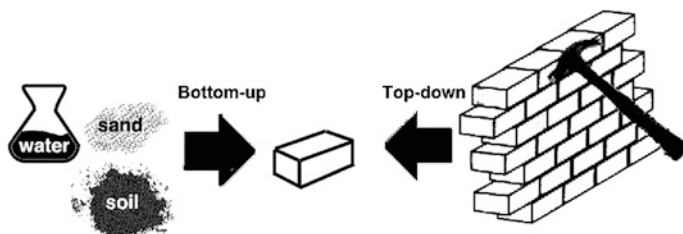


Fig. 2 Illustration of the concepts of *Bottom-up* and *Top-down* methods

Bottom-up production of nanomaterials is divided into the following categories: gaseous phase, liquid phase, solid phase, and biological methods. Among others, chemical vapor deposition and atomic layer deposition belong to the gas-phase methods whereas reduction of metal salts, sol-gel processes, templated synthesis, and electrodeposition correspond to liquid-phase methods [10].

Due to the numerous scientific articles published in the field of synthesis of silver nanoparticles; in this chapter we have focused on providing a rationalized view of some of the available synthetic methods to obtain silver nanoparticles, mostly bottom-up, in liquid phase, excluding biological and microbiological synthesis as reported elsewhere [11, 12].

The main aim of this contribution is to provide guidance when choosing a synthetic method to prepare AgNP for a giving application. Mechanistic insights to understand why some factors would affect the synthetic outcome are also discussed in this chapter.

Although some reviews on synthetic procedures for the preparation of AgNP are reported in literature [13–15], only a few have focused on mechanistic features. In this chapter, we present a systematic review of the mechanism(s) involved in the synthesis of AgNP in the hope “to light up the black box.” Further, in the end of this chapter, we have included a summary and a table containing the most commonly used characterization techniques and the information obtained from them.

2 Chemical Reduction

Reduction of the corresponding metal cation represents a straightforward reaction to obtain metal nanoparticles. The key relays on selecting the right parameters that permits control over the synthesis outcome, and so a good understanding on the mechanism is required.

Generally, these reactions are carried out in solution and the product has colloidal characteristics. For this reason, the common term used for the overall phenomenon is co-precipitation, that involves the concurrence of different phenomena; reduction, nucleation, growth, coarsening, and/or agglomeration [16]. The way these processes take place is, in fact, the mechanism of the synthesis.

As for any redox reaction, the values of the standard reduction potentials (E^0) determine the pairs of reactants required for successful chemical conversion. This means that the free energy change in the reaction, ΔG^0 , must be negative, or what is equivalent $\Delta E^0 > 0$. Thus, in the case of silver, the relatively large electropositive reduction potential of $\text{Ag}^+ \rightarrow \text{Ag}^0$ in water ($E^0 = +0.799$ V, [17]) permits the use of several reducing agents e.g., sodium citrate ($E^0 = -0.180$ V, [18]), sodium borohydride ($E^0 = -0.481$ V, [17]), hydrazine ($E^0 = -0.230$ V, [16]) and hydroquinone ($E^0 = -0.699$ V, [19]). Next, we will look at a few examples more in detail.

2.1 Reduction by Citrate Anion

In 1951, Turkevich [20] reported the synthesis of gold nanoparticles in aqueous solution at boiling temperature using sodium citrate to reduce AuCl_4^- . Since then, this methodology, known as the Turkevich's method, has been extended to other metals such as the case of silver [3, 21].

Lee and Meisel [3] prepared AgNP in water, for SERS applications, using the described method but in that particular case no insight into the mechanism or full characterization of the AgNP (size and shape) was given. Nevertheless, a few years later, researchers became more interested on elucidating the actual mechanism involved in the whole process in order to gain more knowledge on what parameters really matter and how it will be possible to achieve better reproducibility between batches, and also size and shape control.

From the pioneering studies [3, 20], it is now known that citrate acted both to reduce the metal cation and stabilize the resulting nanoparticles. Also, it was believed that this reactant played a role on determining the growth of the particles. Pillai and Kamat [21] investigated the action of citrate on controlling the size and shape of AgNP. They found that by using the boiling method at different citrate concentrations, AgNP with plasmon maximum absorbance at 420 nm were produced. By increasing the relative concentration of sodium citrate to silver cation i.e. $[\text{Citrate}]/[\text{Ag}^+]$ from 1 to 5 times, the elapsed time for formation of AgNP was reduced from 40 to 20 min, respectively, indicating that under equimolar conditions a fraction of the Ag^+ was not reduced.

In order to learn more about the function of citrate as stabilizer, $\text{SiO}_2@\text{AgNP}$ were synthesized using NaBH_4 and after the addition of sodium citrate, where the formation of $\text{SiO}_2\text{-Ag-citrate}$ complex with an association constant of 220 M^{-1} between citrate and the silver colloids was confirmed [21].

In addition, synthesis studies of AgNP by reduction with pulse radiolysis proved that citrate anions act at early stages by complexing Ag_2^+ dimers, and so modulating the particle growth [21]. In fact, the absorbance maximum of the plasmon obtained with this method was found $\approx 400 \text{ nm}$, a 20 nm blue shifting of the value observed for the AgNP obtained by classical Turkevich's method, indicating that different mechanism of growth particle is operating depending on the reduction method. This interaction had also been observed earlier by Henglein and Giersig [22] in their work on the capping effect of citrate on AgNP prepared by radiolytic reduction.

As a consequence of the slow rate in the citrate reduction method, there is an evident contribution of this reactant to obtain larger AgNP (50–100 nm) [21]. In other words, once the first particle seeds are formed from the Ag^+ reduction by citrate, the remaining anion can complex to the metal surface decreasing the total amount of citrate available in the bulk to further reduce more Ag^+ . Thus, fewer new seeds are formed and the initial particles begin to grow via Ostwald ripening, in which the larger particles grow at expense of the smaller ones. Therefore, more time is needed to complete the reduction reaction when using this method. Figure 3 illustrates this process.

Addition of glycerol (40 % V/V), a highly viscous solvent ($\eta \approx 1,400 \text{ cp}$ [23]), to the aqueous medium reduced polydispersity ($\approx 5 \%$) and permitted size control

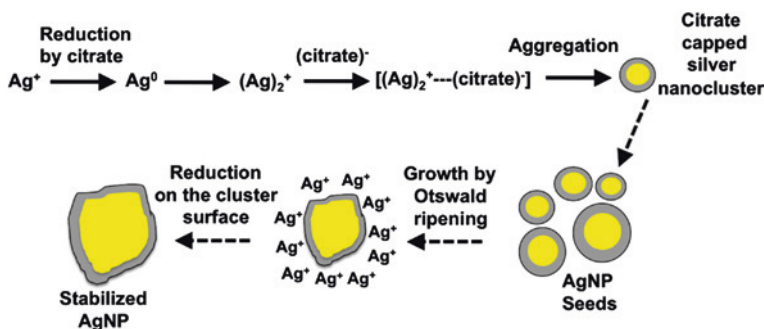


Fig. 3 Representation of the nucleation and growth mechanisms for AgNP obtained by the citrate method according to Ref. [21]

(30 nm) without affecting the spherical shape [24]. Reduction and/or nucleation rates are slower as evidenced by the delayed appearance of the characteristic yellow colour for AgNP, accordingly with expected for diffusion processes in viscous solvents. Although the effect of glycerol on the AgNP synthesis is not fully understood, it is believed that glycerol protects the AgNP against further ripening [24].

The presence of different amounts of NaOH during the synthesis by citrate reduction was found to redirect the reaction to the production of crystalline silver nanowires [25]. These Ag nanostructures were characterized by TEM (observing wires up to 12 μ long), X-ray energy dispersive microanalysis and UV-vis spectroscopy in which a sharp absorption at 370 nm corresponding to the transverse plasmon was observed. The effect of NaOH in the outcome of the synthesis was attributed to interference of hydroxide with the association and capping ability of citrate with silver [25].

2.2 Reduction by NaBH_4

First attempts to elucidate the mechanism of AgNP synthesis using sodium borohydride (Eq. 1) as the reducing agent were made by Van Hyning and Zukoski [26]. Following the reaction progress ‘in-situ’ by UV-vis spectroscopy and ‘ex-situ’ by Transmission Electron Microscopy (TEM) they were able to infer that the nucleation and growth mechanisms for these nanoparticles do not follow the La Mer’s model [27, 28] (Fig. 4), rather it was dependent on colloidal interactions [26]. Recently, Polte et al. [29] proposed a better description of the AgNP formation pathway and the relevant factors to obtain size-controlled AgNP based on a rational design [29].



From time-resolved synchrotron small-angle X-ray scattering (SAXS) and UV-vis spectroscopy measurements combined with TEM characterization, a four-step growth mechanism for the AgNP synthesis by reduction with NaBH_4 was proposed (Fig. 5) [29].

Fig. 4 Representation of La Mer's model for nucleation and growth [27, 28]. C_s , C_{min} and C_{max} are solubility concentration, minimum and maximum concentration to start nucleation, respectively

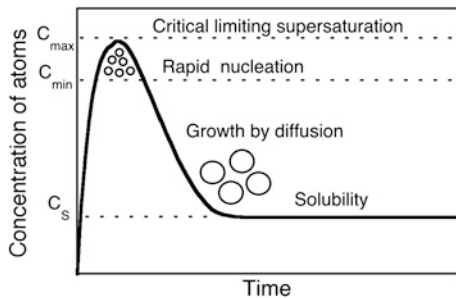
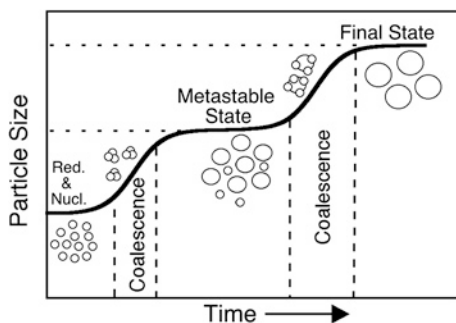
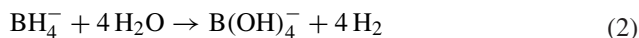


Fig. 5 Illustration of the growth mechanism for AgNP synthesized using NaBH_4 as proposed by Polte et al. [29]



The first step involves reduction (<200 ms) of Ag^+ to Ag^0 atoms. These atoms form dimers, trimers, etc. clusters. In a second stage (≈ 5 s) the clusters coalesce to generate small particles with a radius of 2–3 nm. This step is followed by a metastable state, where the particles maintain a constant size for around 5–10 min. After this period, a second and last coalescence phase takes place (within 30–60 s) to render the final AgNP with an average size of 5–8 nm (Fig. 5) [29]. A detailed study of the metastable state and final coalescence phase by time-resolved SAXS showed that colloidal stability during the intermediate state is enough to prevent further growth due to particle aggregation [30]. Note that each coalescence process implies an aggregation process as a consequence of a decrease in particle stability. Then, it was proposed that the total consumption of BH_4^- is a triggering event for the initiation of the second coalescence phase due to loss of stability plausible by oxidation of the metal surface [30]. Although the reaction stoichiometry with Ag^+ is usually 1:1, BH_4^- is added in excess. Therefore, the extra borohydride anion remains in solution helping to stabilize the formed nanoparticles (electrostatic stabilization), but it will also begin to hydrolyze according to the following simplified Eq. (2), decreasing the available borohydride ion. Hydrolysis is slower compared to the reductive reaction, becoming the dominant process once all the metal cations are reduced.



Another phenomenon that takes place is the partial oxidation of the metal nanoparticle surface forming silver oxides. The presence of these oxides decreases the electrostatic stabilization of the AgNP provoking in consequence their aggregation. When there is still BH_4^- left in solution, the oxidation of the particle surface can be reversed, avoiding the aggregation process but once all BH_4^- is consumed, there is green light to start the final coalescence stage until the stable size is obtained [30].

The addition of a bulky stabilizing agent such as polyvinylpyrrolidone (PVP) to the reaction medium does not change the growth mechanism (the final size is indeed the same as without PVP) but affects the duration of each step and decreases the polydispersity (15–20 %) [29].

Based on a better understanding of the growth mechanism, Wuthschick et al. [30] were able to obtain reproducible sizes (between 4 and 8 nm) between different batches by controlling the $\text{BH}_4^-/\text{B(OH)}_4^-$ ratio, without the addition of any external stabilizing agent. It was found that a proportion of 32.5 % BH_4^- at the beginning is similar to start the synthesis from the metastable state (Fig. 5), and so the four-step mechanism is reduced to a two-step. Consequently, as the growth mechanism is simplified a good control over the final size is gained.

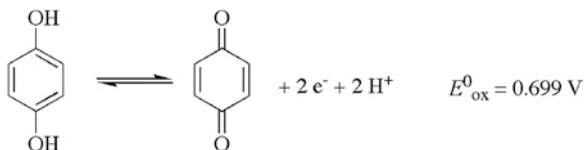
In summary, using a strong reductant, like NaBH_4 ($E_{\text{red}}^0 = -0.481 \text{ V}$, [17]), results in a faster reduction of Ag^+ than the growth process. The growth mechanism is governed by coalescence closely related to the electrostatic stabilization of the nanoparticles. Classical models for nucleation and growth processes (like La Mer's) do not apply in this case.

2.3 Reduction by Hydroquinone

Oxidation of Hydroquinone (HQ, Scheme 1) involves a two-electron transfer and loss of two protons producing *p*-benzoquinone [19]. According to the above-mentioned redox potential, HQ is able to reduce Ag^+ to obtain AgNP.

Nucleation and growth of AgNP obtained using HQ have been studied by UV-spectroscopy combined with TEM and titration microcalorimetry [31, 32]. Pérez et al. [31] observed a strong dependence on the size and morphology of AgNP with the concentration of HQ at early stages of reaction. A high local concentration of HQ induces more nucleation sites whereas a low local concentration of the reducing agent favors growth over nucleation. Consequently, a protocol involving addition of a concentrated solution of HQ to the reaction medium yields AgNP with smaller sizes (10–30 nm). On the other hand, a protocol in which a diluted solution

Scheme 1 Two-electron oxidation of Hydroquinone to *p*-Benzoquinone



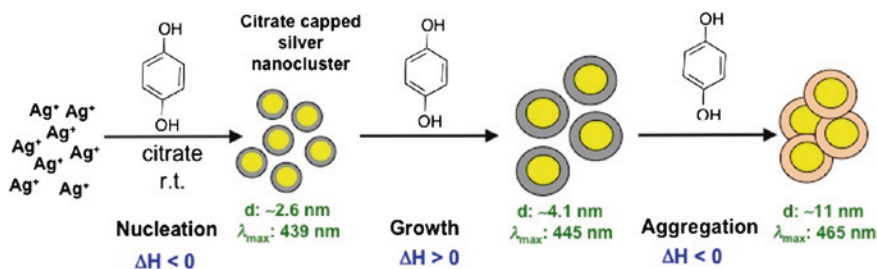


Fig. 6 Illustration of the growth mechanism for AgNP synthesized using HQ at room temperature as proposed in Ref. [32]. Change color in NP shell indicates HQ replaced citrate as capping agent

of HQ is added to the reaction yields larger and more polydisperse AgNP with sizes up to 200 nm. The previous observations are valid for AgNO_3 as precursor, where it can be assumed that Ag^+ is completely solvated in solution. Nevertheless, when Ag^+ is complexed as in $[\text{Ag}(\text{NH}_3)_2]^+$ with the presence of counter ions as Cl^- , the growth is arrested independent on the protocol followed, monodispersity raises and small quasi spherical particles of $\sim 14 \text{ nm}$ are predominantly obtained. This effect has been attributed to an unfavorable adsorption of the metallic precursor onto the metal surface, then the growth by further reduction of Ag^+ on the AgNP surface is quenched [31].

Isothermal titration calorimetry (ITC) studies on the formation of AgNP, starting from AgNO_3 and hydroquinone in the presence of sodium citrate as stabilizer, reports that the growth mechanism follows a three-step mechanism (Fig. 6). First, reduction of Ag^+ by HQ to get silver clusters ($\sim 2.6 \text{ nm}$, $\lambda_{\text{max}} = 439 \text{ nm}$) takes place. This nucleation phase is an exothermic (favorable) process that is followed by a growth phase of endothermic nature to reach sizes of $\sim 4.1 \text{ nm}$ ($\lambda_{\text{max}} = 445 \text{ nm}$) and finally, if aggregation of AgNP occurs the process is again exothermic with final nanostructures around 11 nm in size ($\lambda_{\text{max}} = 465 \text{ nm}$) [32]. This latter process occurs with further addition of HQ that is likely to be replacing citrate from the NP surface and thus, decreasing stabilization due to electrostatic repulsion.

2.4 Reduction by Gallic Acid

Reduction of Ag^+ in water at room temperature can also be accomplished using gallic acid (GA) whose oxidation potential is 0.5 V (Scheme 2). Besides the redox potential value, the presence of hydroxyl groups in the benzoic acid structure at determined positions plays an important role in the synthesis of metal nanoparticles. For example, the generation of nanoparticles was not successful when using benzoic acid derivatives substituted by hydroxyl groups at *meta* positions but are obtained when the hydroxyls are located at *orto*- and

Scheme 2 Two-electron oxidation of gallic acid to the quinone form [33]

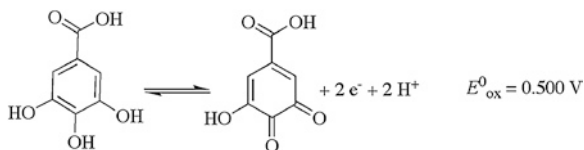
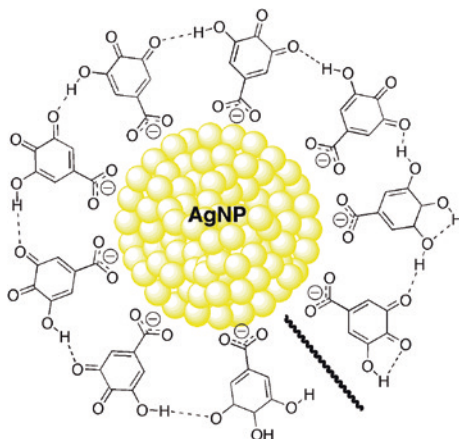


Fig. 7 Illustration of the stabilized capped-AgNP synthesized using GA as proposed in Ref. [33]



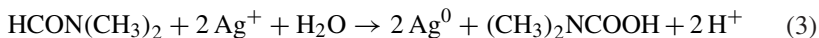
para positions [33]. Note that the hydroxyls are the reactive part (Scheme 2) and the carboxylic group acts as the stabilizing part (Fig. 7). The need of having hydroxyls at the mentioned positions can be explained by the formation of a network of the capping molecules around the particle, held by hydrogen bonding interactions between the surface molecules (Fig. 7), that increases the colloidal stability (zeta potential; $\xi = -45$ mV) [33]. Moreover, addition of NaOH is necessary to obtain the silver colloids [33]. Then, the silver species reacting could be Ag_2O that has been recently reported as a good AgNP precursor by thermal decomposition [34].

2.5 Synthesis of AgNP in Organic Solvents

Most reported examples of AgNP obtained by chemical reduction are performed in aqueous media [35–37]. A post-synthesis transfer to an organic solvent is usually difficult due to aggregation processes. Nevertheless, the synthesis of metal nanoparticles in organic solvents has some advantages such as high yield and narrower size distribution, with the additional advantage that in some cases the solvent itself can act as reducing agent to obtain AgNP [14].

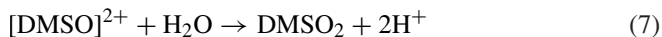
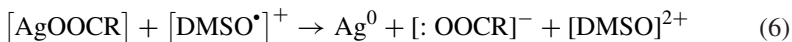
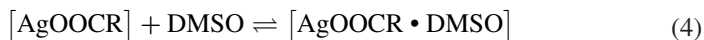
For example, Pastoriza-Santos and Liz-Marzan [38] proposed a synthetic route to obtain AgNP spheres (≈ 6 –20 nm) from the spontaneous reduction of silver

nitrate by dimethylformamide (DMF) and using 3-(aminopropyl)trimethoxysilane (APS) to stabilize the particles. The overall reaction displayed in Eq. 3 shows the formation of a carbamic acid that together with the resulting acidic environment promote the deposition of silica shells onto the formed particles [38]:

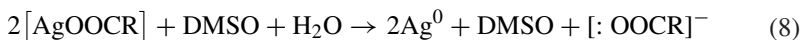


Reaction rate, size and monodispersity of the nanostructures can be controlled by variation of temperature from room to boiling temperature. Increasing the temperature accelerates the silver reduction favoring silica polymerization directly onto the APS-coated silver particles surface. Thus, at 156 °C APS-capped AgNP around 19 nm are obtained [38]. Replacing the stabilizing agent APS by polyvinylpyrrolidone (PVP) favors the formation of nanoprisms by choosing the right experimental conditions (concentration of reactants and reflux time) [39].

Another reported synthetic route was performed in dimethyl sulfoxide (DMSO) at room temperature. Quasi-spherical AgNP (4.4 nm) were obtained from the spontaneous reduction of silver 2-ethylhexanoate [Ag(ethex)] by DMSO [40]. Increasing the temperature accelerates the reaction. Based on experimental data and ab initio calculations a mechanism for this reaction has been proposed and it is shown as follows (R is—(C₂H₅)CH(CH₂)₃CH₃ in Eqs. 4–7):



The overall reaction can be written as follows (Eq. 8).



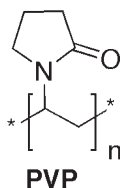
Note that in the first step (Eq. 4) the formation of a complex between Ag(ethex) and DMSO is proposed which was supported by testing that the reaction does not occur with other silver salts such as AgNO₃ and AgClO₄ otherwise 2-ethylhexanoate is present in the reaction medium. In addition to that, ab initio calculations showed that the complex [Ag(DMSO)ethex] has an adequate LUMO energy and low energy difference between HOMO-LUMO gap what is consistent with a good precursor for reduction [40].

In order to overcome the instability of the synthesized AgNP dispersions by this way, it is necessary to use capping molecules to gain stability. The best capping agent used was sodium citrate (see Sect. 1).

A deeper analysis of the synthesis of AgNP in organic solvents with focus on rationalizing the nucleation process to engineer the final outcome can be found in a tutorial review by Sun [14].

2.6 Polyol Method and Shape-Controlled Synthesis

Although the polyol method can also be considered as a case of synthesis in organic solvents [14, 41, 42], the versatility that provides to obtain AgNP with different morphologies makes this method relevant to be analyzed separately.



Briefly, polyol synthesis involves the reduction of a metal salt used as precursor by a polyol, usually ethylene glycol (EG) at an elevated temperature ($\approx 160^\circ\text{C}$ for EG), and in order to prevent agglomeration of the particles a capping agent commonly used is PVP [4, 43–45]. EG (as other polyols) probably oxidizes to aldehyde species with an oxidation potential of 1.65 eV [46]. Reduction power of EG is markedly dependent on the temperature, giving the ability to control the nucleation and growth processes by choosing the reaction temperature [47]. Another advantage is that the polyol can serve as both solvent and reducing agent.

Before analyzing the reasons for shape control during the synthesis by the polyol method, it is important to note the critical role of PVP in the stability, size and shape uniformity of AgNP. From infrared (IR) and X-ray photoelectron spectroscopy (XPS) it was inferred that the oxygen and nitrogen atoms of PVP can promote the adsorption of this polymer chains onto the metal surface [36]. In addition, PVP interacts more strongly with silver atoms located in the $\{100\}$ facets than those on the $\{111\}$ (lower energy facets) [42].

La Mer's model (Fig. 4) seems to explain at some extent the nucleation and growth mechanisms [14, 36], taking place in the polyol method though it still represents an oversimplified view of the nucleation process [14]. That said, we now summarize different examples of shape control: nanocubes, nanowires and nanospheres.

TEM studies performed on small silver nanoparticles demonstrated that there is a good probability that morphology fluctuates between the kinetically stable single crystal (sc) and the thermodynamically stable twinned (tw) particles during earlier stages of growth [44]. This fact supports a model where morphology in small particles ($<5\text{ nm}$) is exchanged between sc and tw induced by thermal

fluctuations, with multiply twinned decahedra (MTP) being the most abundant shape. Thus, it is understood that a common NP synthesis outcome results to be a mixture of single crystals and twinned particles as shown in Fig. 8 [44]. It also has been proposed that sc seeds lead to obtaining truncated cubes and tetrahedrons as final shapes while tw seeds conducts to rods, wires and spheres depending on the reaction conditions [47].

Experimental conditions that favor fast nucleation and fast growth like a high AgNO_3 concentration (0.125–0.25 M) and low PVP to Ag^+ ratio (≈ 1.5), promote the formation of nanocubes as the possibilities to get twinned particles diminished. Then, the most abundant structures between the pristine particles are single crystals that follow their growth assisted by PVP to reach the final shape of truncated cube. Figure 9

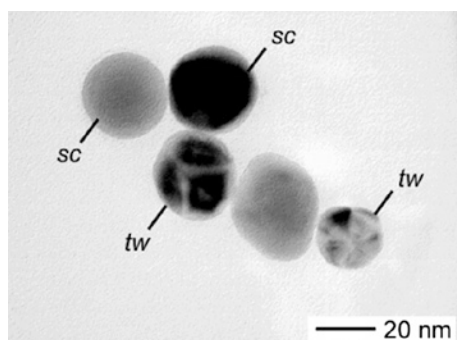


Fig. 8 TEM images showing a mixture of single crystal and twinned morphologies after 2 h reaction for AgNP synthesized by the polyol method. Reprinted with permission from Ref. [44]. Copyright © 2004 American Chemical Society

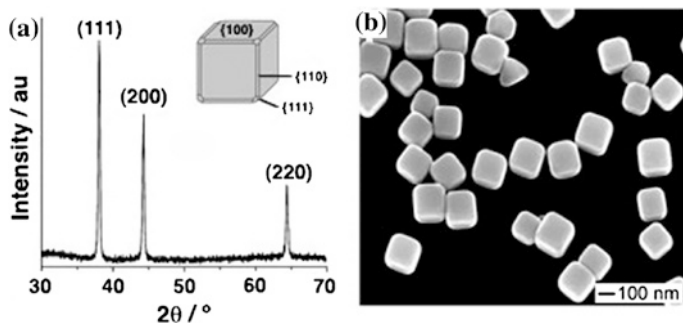


Fig. 9 **a** X-ray diffraction (XRD) pattern obtained from silver nanocubes, synthesized by the polyol method from AgNO_3 (0.25 M) with a PVP to Ag^+ ratio of 1.5, deposited on a glass substrate. Peaks are assigned to diffraction from the {111}, {200} and {220} planes of silver. Inset shows the drawing of one cube indicating the corresponding crystallographic planes. **b** SEM image of the same silver nanocubes showing the slightly truncated corners and edges of each cube. Reprinted with permission from Ref. [47]. Copyright © 2005 WILEY-VCH Verlag GmbH&Co. KGaA, Weinheim

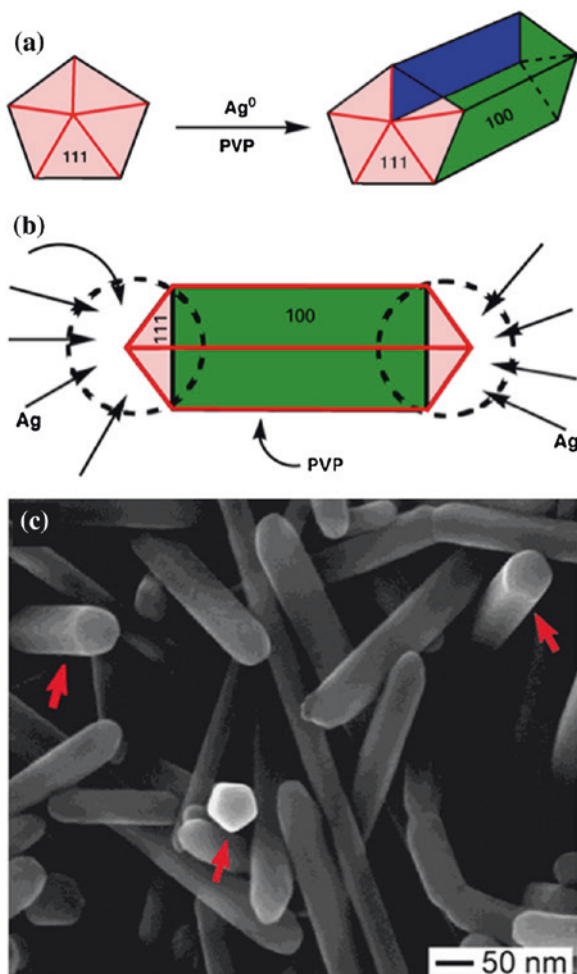


Fig. 10 **a** Representation of the evolution of a nanorod from a decahedral silver particle with the assistance of PVP by the polyol method. The ends of this nanorod are terminated by {111} facets, and the side surfaces are bounded by {100} facets. The green color indicates the preferential adsorption of PVP on the {100} facets, and the pinkish color stands for the weaker interaction with the {111} facets. The red lines on the end surfaces represent the twin boundaries that can serve as active sites for the addition of silver atoms. The plane marked in blue shows one of the five twin planes that can serve as the internal confinement for the evolution of nanorods from MTP. **b** Representation of the diffusion of silver atoms toward the two ends of a nanorod, with the side surfaces completely passivated by PVP. This drawing shows a projection perpendicular to one of the five side facets of a nanorod, and the arrows represent the diffusion fluxes of silver atoms. **c** SEM image of silver nanowires obtained by the polyol method. The red arrows indicate cross-sections of the nanowires showing pentagonal cross-sections. **a–c** were adapted with permission from Ref. [42]. Copyright © 2003 American Chemical Society

shows the silver truncated nanocubes (average edge length: 175 nm) obtained by the described polyol method from AgNO_3 (0.25 M) [47].

On the other hand, if the AgNO_3 concentration is reduced to 0.085 M while the PVP: Ag^+ ratio is kept constant (1.5) and the reaction temperature is above 110 °C the resulting particles are nanowires. The most accepted explanation for this result is that these conditions promote a high yield in MTP (decahedral) during early growth stages. Then, new Ag^0 are more likely to crystallize on the highly reactive twin defects of the decahedral. In the presence of PVP, the {100} sides are passivate due to its preferentially adsorption on this facets. For that reason, further growth takes place in the {111} direction to reach the final nanowires shape (Fig. 10) [42, 46, 47].

In order to overcome the growth in a particular direction due to passivation of a specific facet, it is necessary to increase the PVP: Ag^+ molar ratio more than three times. In that way, the entire particle surface is covered by PVP and seeds are prone to follow an isotropic growth to end as mostly spherical in shape [47].

3 Light-Assisted Methods

The first reports on the effect of light on the transformation of some metal salts were written in the 18th century, when the German scientist Johann Schulze (1687–1744) discovered that silver salts darken by irradiation of light, initiating the development of photography, although the concept of nanomaterials had to wait almost 200 years.

In the last decades, light-assisted methods for NP preparation have been largely developed as well, basically due to the versatility and selectivity of photochemical reactions to generate in situ the reducing species with high spatial resolution and almost no modification of the surrounding media. The fundamentals and applications of different light mediated methodologies have been recently reviewed [13, 15, 48]. As we mentioned in a general manner in the introduction, photo-induced synthetic strategies can be also categorized into top-down (photophysical methods) and bottom-up (photochemical methods) approaches.

3.1 Photophysical Methods

AgNP are prepared via subdivision of bulk silver metal usually by laser ablation methods [49–51]. As example, the influence of anionic surfactant molecules $\text{C}_n\text{H}_{2n+1}\text{SO}_4\text{Na}$ ($n = 8, 10, 12, 16$) on the stability of AgNP produced by laser ablation of a metal silver plate with a pulsed Nd-YAG laser operating at 532 nm (10 ns full width at half maximum (fwhm), <90 mJ/pulse, 10 Hz) [49]. The stability of the AgNP capped with the anionic surfactant was modulated by the surfactant coverage and the charge state on the nanoparticle surface. The AgNP tend to aggregate when the

coverage degree is less than unity, while they are very stable when the particle surface is covered with a double layer of the surfactant due to the electrostatic repulsion forces. Moreover, more efficient stabilization was obtained by surfactant with a longer hydrocarbon chain due to larger hydrophobic interactions between them [49].

Additionally, the effect of sodium chloride (NaCl) on the morphology and stability of AgNP generated by laser ablation (Nd:YAG 1,064 nm) was analyzed [50, 51]. The increment in NaCl concentration up to 5 mM in aqueous solutions produced AgNP with average size of ~26 nm, but with a continuous decrease of the full width at the half maximum (fwhm) of the plasmon absorbance band centered at 400 nm, together with the simultaneous increase of the absorbance signal. However, above that NaCl concentration the absorbance of the plasmon was smaller and the fwhm value slightly increased. The salt effect was inherent with the growth phase of the AgNP during the ablation of the bulk silver surface, since no effect on the plasmon band was observed when NaCl was added to AgNP in water previously prepared by laser-ablation. It was concluded that the presence of Cl^- ions provides reduction of nanoparticles size and increases the efficiency of formation of AgNP by laser irradiation of the silver target immersed in water. However, the long-term stability (i.e. >20 days) of the AgNP was reduced by the Cl^- ions [50].

In another case, stable suspensions of AgNP were prepared by laser-ablation of a highly pure (99.99 %) silicon (Si) target immersed in aqueous solution of AgNO_3 as silver source [52]. The third-harmonic ($\lambda = 355$ nm) beam of a Q-switched Nd:YAG laser was focused on the Si target and the effects of the salt concentration and irradiation time were evaluated. The maximum plasmon absorbance at 400 nm was obtained using 0.125 mM AgNO_3 solutions, with the formation of spherical AgNP with average diameter of ~11 nm. Above this concentration, the plasmon absorbance was less intense, red-shifted and broader indicating that under these salt concentrations AgNP with larger diameter and a broad size distribution were formed [52].

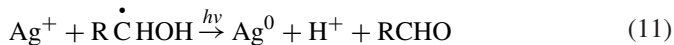
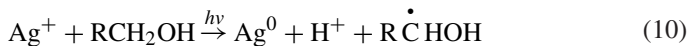
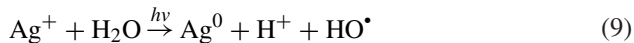
3.2 Photochemical Methods

Regarding to the photochemical methods for metal NP preparation (bottom-up approach), they are based on the reduction of the metal cation M^{n+} to M^0 either by direct or indirect (photosensitized) photolysis.

Direct photoreduction has been established as an important technique for metal NP synthesis, where M^0 is formed through the direct excitation of a metal source, normally a salt. Due to the advantage of being free from reducing agents, it has been widely employed in the various mediums including polymer films, glasses, cells, etc. [15].

Direct photoreduction of silver perchlorate (AgClO_4) in aqueous and alcoholic solutions by irradiation with UV-light at 254 nm was investigated in the 70s by Hada et al. [53]. The photoreduction mechanism is based on the electron-transfer

from a solvent molecule to the electronically excited state of Ag^+ to form Ag^0 (Eqs. 9–12):



The reactivity, and therefore the quantum yield of formation of AgNP, was strongly increased in the presence of α -alcohols, due to the easier abstraction of the labile α -hydrogen. The formed radical also reduced Ag^+ (Eq. 11) accelerating the production of AgNP [53].

Long term stable (~ 6 months) AgNP were obtained by photoreduction of $[\text{Ag}(\text{NH}_3)_2]^+$ aqueous solution with PVP as both reducing and stabilizing agent [54]. Following the increment in the surface plasmon absorption maxima at 420 nm the formation of AgNP was monitored. It was found that the plasmon absorption intensity increased with PVP concentration as well as the maximum absorption wavelength (λ_{max}) was blue shifted. Transmission electron microscopy (TEM) showed the resultant particles were 4–6 nm in size with uniform particle size distribution. Huang et al. [55] also reported the synthesis of AgNP employing the photoreduction of AgNO_3 solutions with 254 nm UV irradiation in the presence of PVP as protecting agent.

Finally, a marked interest in UV photoreduction of silver salts embedded in polymeric films and/or inorganic hydrogels for in situ generation of AgNP exists [56–58]. Fast generation of AgNP was observed when fibers of polymer blends of poly(vinyl alcohol) (PVA) and poly(acrylic acid) (PAA) crosslinked with DMSO were irradiated with 350 nm light. Initially, small AgNP clusters were formed, which were stable in the dark but transformed into larger metal particles upon further illumination [56]. The formation of AgNP by UV photoreduction of AgNO_3 in layered laponite suspensions without any addition of reduction agent or heat treatment. Relatively larger sized (40–110 nm) AgNP were obtained, but with extremely long-term stability, opening the application of the hydrogel as antibacterial agent [57].

Thin films of PAA embedded with AgNP prepared by UV photoreduction exhibited cyclically changeable optical absorbance properties (spectral shift) during variation of pH of aqueous medium [58]. The phenomenon was attributed to conformational changes in the polymer matrix induced by pH changes, which leads to variation in the 3D configuration of the AgNP ensemble by reversible modification of the inter-particle distance during swelling and shrinking processes within the PAA matrix (Fig. 11). These changes result in the reversible blue-red shifting of the

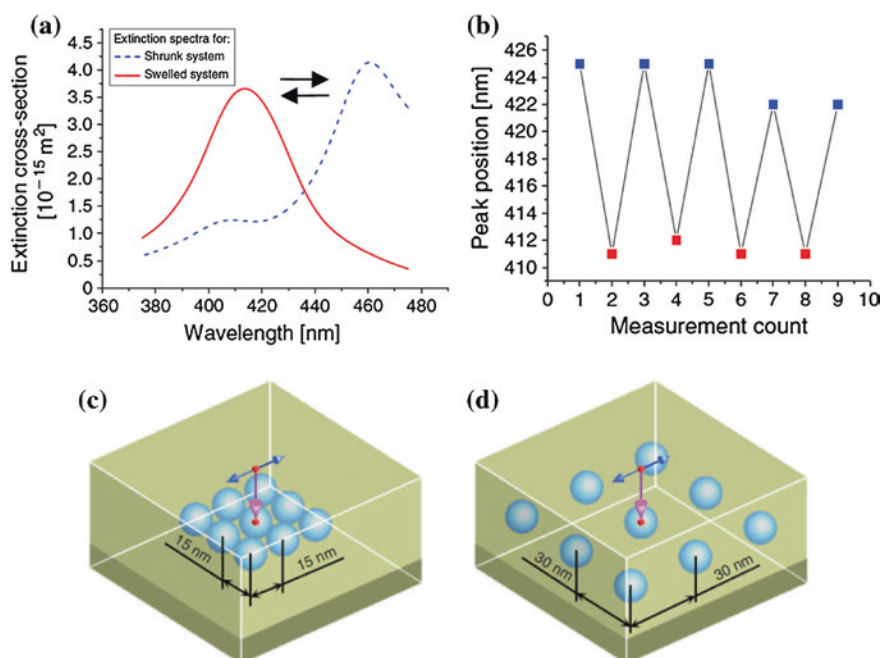


Fig. 11 **a** Electronic absorption spectra of AgNP obtained by direct photoreduction in PAA hydrogel film wet with 0.1 M H_2SO_4 (swelled system) and with deionized water (shrunk system). **b** Absorbance spectrum peak positions after 10 cycles of alternating immersion where red and blue squares indicate the swelled and shrunk systems, respectively. **(c–d)** Models of the shrunken **(c)** and swollen **(d)** states of the PAA hydrogel containing AgNP. Adapted with permission from Ref. [58]. Copyright © 2012 CSIRO Publishing dx

plasmon band absorption maximum, with the possibility of using this “molecular memory” in the development of optoelectronic devices and sensors [58].

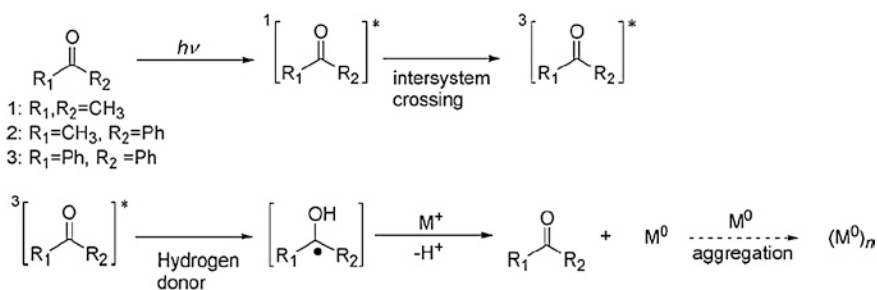
As despited above, the general mechanism of NP formation by direct photoreduction of the metal cation is usually by a solvent-assisted disproportionation process that depends on the nature of the precursor metal. However, in most cases, the use of UV excitation source is necessary in direct photoreduction since most of metal cations and/or metal salts only absorbs in this spectral region. This issue can represent a very important experimental limitation, since UV-light sources are more expensive and not always easily available. Moreover, many molecules used as stabilizing agents can also absorb in the UV, acting as inner filter of the excitation beam.

Nevertheless, this limitation can be overcome by photosensitized synthesis of NP. In this case a sensitizer molecule (organic dye, aromatic ketones, polyatomic anions) that can absorb UVA-visible light (320–700 nm) generates reducing intermediates (free radicals, anions, solvated electrons, etc.) that react with the M^{n+} co-existing in the solution to form the M^0 [15].

Photosensitized methods are based either on the formation of reactive excited states or the photogeneration of organic radical species from the sensitizer molecule [15]. In this chapter we will focus on the photosensitized generation of AgNP mainly by ketyl radical formation either by hydrogen abstraction or bond cleavage as a very useful strategy for AgNP preparation by indirect photolysis [15, 59].

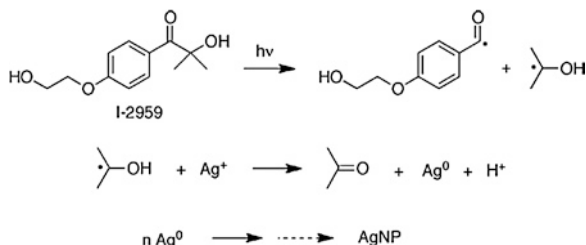
Typically, in the former case, an aliphatic or aromatic ketone, such as acetone, acetophenone or benzophenone, is excited with UVA/UVB light ($300 < \lambda$ (nm) < 360) to the singlet excited state, in which by efficient intersystems crossing decays to the long-lived triplet state. Due to the n, π^* character of the ketone triplet excited state it becomes an excellent hydrogen abstractor from appropriated donors (e.g. alcohols, benzylic and allylic hydrogens, some hydrocarbons, etc.) to produce the respective ketyl radical. In the case of alcohols, which in many cases can be used as solvent or co-solvent, the ketyl radical and the radical derived from the alcohol are formed, which are able to reduce the metal cations to generate the NP.

According to Scheme 3, after the formation reaction of M^0 , the ketone is regenerated and a new photosensitization cycle can be initiated by absorption of a UV photon, a significant issue to consider when polyvalent metal cations are reduced since ketyl radicals are one-electron reducing species. Note that the global reaction also produces H^+ , and therefore in non-buffered solutions the solution pH decreases to acidic values (pH ~ 3) [59]. Both Majima's [15] and Scaiano's [59] groups have extensively explored the use of ketone photosensitization process for AgNP synthesis under different conditions and applications. As example, since the primary precursor is the excited triplet state of the ketone, the effect of magnetic field on the formation of AgNP was evaluated [60]. In this case, photoreduction of benzophenone in sodium dodecyl sulphate (SDS) micellar solutions in the presence of Ag^+ produced a very rapid and efficient formation of AgNP, and the process was modulated by external magnetic field by splitting of triplet sublevels as a result of Zeeman effect, even under weak and mild field intensities (up to 120 mT). The amount of AgNP produced was increased with the intensity of the magnetic field with slight modifications in the plasmon absorbance band position and increment of the average particle size from ~ 4 to 8 nm. Therefore, it was concluded that weak magnetic fields, such as those produced by magnetic stirring bars (< 10 mT), can modulate the formation of AgNP by benzophenone photoreduction [60].



Scheme 3 Sensitization mechanism of ketone/hydrogen donor system used for nanoparticle formation. Reproduced with permission from Ref. [15]. Copyright © 2009 Elsevier

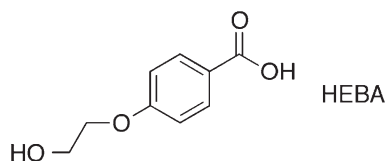
Scheme 4 Mechanism for AgNP formation starting from the photoinduced bond cleavage of Irgacure-2959. Reproduced with permission from Ref. [61]. Copyright © 2013 Springer



Other source of ketyl radical for metal reduction is given by photoinduced bond cleavage reactions of α -hydroxy ketones (benzoin)s, such as the water-soluble 2-hydroxy-4'-(2-hydroxy-ethoxy)-2-methyl-propiophenone (Irgacure-2959[®], I-2959, Scheme 4).

The photochemistry of α -hydroxy ketones has been well characterized and the homolytic rupture of the α -cleavage bond favored by alkylation of the 2-hydroxy group occurs in the picosecond time scale after excitation [62]. The case of I-2959 is remarkable since is commercially available, water-soluble, and produces ketyl radicals with a quantum yield of 0.29 in fast photocleavage from a triplet state with a lifetime of just 11 ns [62]. Scaiano's group, principally, has extensively established the use of this compound as photosensitizer for AgNP preparation in water and organic solvents [48, 61, 63–66]. The methodology is clean, fast, and also allows real-time kinetics monitoring by UV-vis spectroscopy using modular CCD spectrometer devices, as shown in Fig. 12 for the formation of AgNP upon steady-state irradiation at 320 (± 10 nm) of 0.2 mM AgNO₃ and 0.2 mM I-2959 in the presence of 1 mM sodium citrate aqueous solutions, together with the TEM image of the final AgNP (average diameter ~ 10 nm) and the yellowish color of the solution due to the strong plasmon absorbance at 404 nm (courtesy of V. Rey, Universidad Nacional de Santiago del Estero).

Finally, it should be noticed that the final fate of the substituted benzoyl radical formed after homolytic bond scission in the first reaction of Scheme 4, is the formation of the corresponding carboxylic acid 4-(2-hydroxyethoxy) benzoic acid (HEBA) that, through mild binding, contributes to the stability of “naked” (without extra stabilizers) metal nanoparticles [48].



At this point, it is worth commenting on the noticeable effect of light on the morphology of the AgNP during the growth stage of Ag⁰ seeds [13, 36, 51, 64, 67, 68]. In general terms, the observed effect is that depending on the excitation wavelength (~ 400 – 700 nm) from lasers, lamps or light emitting diodes (LEDs) illumination sources during the ripening of small spherical AgNP (< 5 nm) seeds,

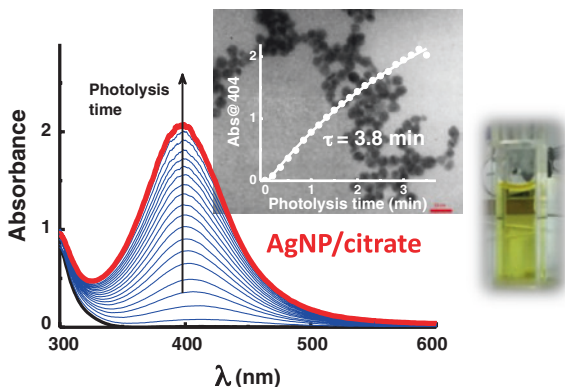


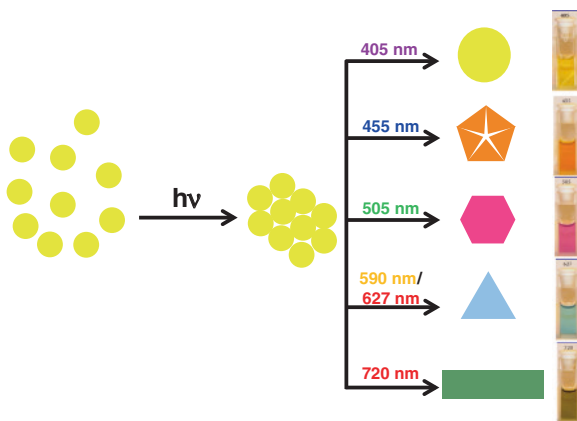
Fig. 12 Absorption spectra of AgNP produced by using I-2959 as photosensitizer showing the formation kinetics. Inset shows the absorbance dependence over photolysis time monitored at 404 nm together with a TEM image and regular photograph of the final AgNP solution. Reaction performed with continuous UV light irradiation in the presence of citrate anions as stabilizer. Courtesy of Dr. Valentina Rey, LACIFO-UNSE, Argentina

different nanostructures with shape and size control, including larger spheres, dodecahedra, nanoplates, and nanorods are photogenerated (Fig. 13).

This striking size and shape control on AgNP formation is associated with the fact that the electromagnetic (EM) field generated in the vicinity of AgNP is extremely high in comparison with other metals.

In summary, light-assisted preparation of AgNP is a very promising field because of the large versatility, selectivity and relatively easier control on shape and size of matured AgNP without need of harsh reaction conditions, such as boiling temperature, etc. These mild reaction conditions also allow NP preparation

Fig. 13 Representation of the photoinduced aggregation/coalescence mechanism that leads to morphology transformation of AgNP seeds according to Ref. [68]



with different labile or biological protecting agents, such as proteins. The current commercial availability of UVA-vis high power LEDs can allow inexpensive preparation of matured AgNP with modulated shape and size for different desirable applications.

4 Electrochemical Methods

Considering that the primary step for AgNP preparation is the one-electron reduction of Ag^+ cation, electrochemical reduction to generate metallic particles seems to be a suitable choice method [69–79].

Synthesis of AgNP by electrochemical reduction was presented by Rodríguez-Sánchez et al. [69], based on the dissolution of a sacrificial silver sheet as the anode (counter electrode), and a sized platinum (Pt) or aluminum sheet was used as cathode (working electrode) and containing tetrabutylammonium salts (TBA bromide or TBA acetate) in acetonitrile as inert solvent. However, AgNP were only obtained using Pt as working electrode. The spherical particles were further characterized by TEM and UV-vis spectroscopy. The increment of the current density was analyzed, observing a size reduction of AgNP from ~7 to 2 nm accompanied by a red shift of the broad plasmon absorption band from 422 to 445 nm. It was observed an oscillatory behaviour by studying various electrochemical parameters and reaction conditions. Characterization by UV-vis spectroscopy showed that the absorption bandwidth of the plasmon band depends heavily on the size and interaction with the surrounding medium, and an autocatalytic stage in the synthesis mechanism was proposed.

Electrochemical synthesis of spherical AgNP (<7 nm) in aqueous media were obtained by using a highly oriented pyrolytic graphite (HOPG) surface modified with a 4-aminophenyl monolayer as counter electrode (Fig. 14) [70]. Changing experimental conditions, such as immersion times, immersion period, and pulse potential time, controlled both the size and number density of AgNP.

Electroreduction of 5 mM AgNO_3 aqueous solutions using a rotating platinum cathode and PVP as stabilizer produces nanospheres with narrow size distribution (~20 nm, SD: 14 nm) which is improved by addition of a surfactant like sodium dodecyl benzene sulfonate (SDBS) (~10 nm, SD: 2 nm) [73]. The dual role of PVP in promoting metal nucleation and circumventing agglomeration of metallic particles allows the formation of small sized metal nanoparticles. Furthermore, by using a rotating platinum cathode, the effective transferring of the electrochemically synthesized NP from the cathode vicinity to the bulk solution is favored, avoiding the occurrence of flocculates in the vicinity of the cathode, and ensuring the monodispersity of the particles [73].

Silver colloidal nanospheres have also been synthesized electrochemically assisted with ultrasonication at 45 °C in a complex media consisting of cyclohexane (100 μL), acetone (100 μL), tetraoctylammonium bromide (0.02 g), hexadecyltrimethylammonium bromide (0.1 g), and ultra-pure water (10 ml) [75]. The average

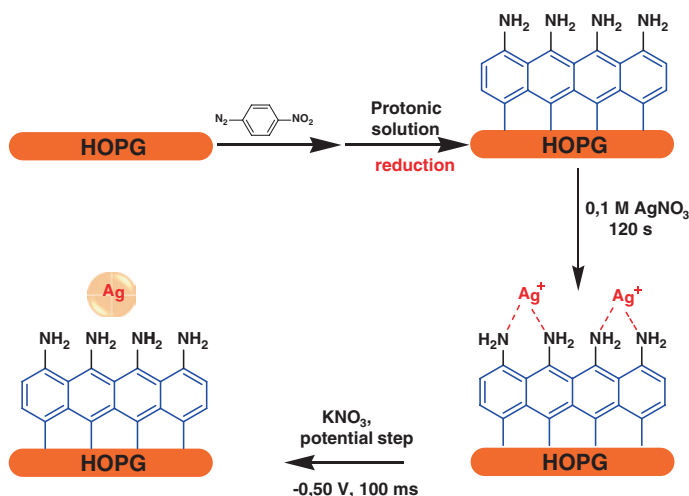
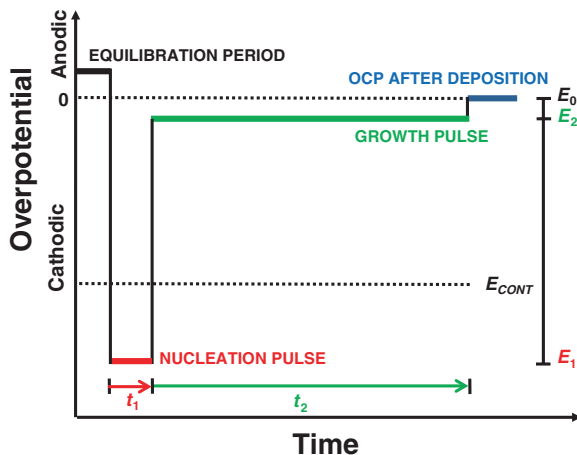


Fig. 14 Illustration of the electrochemical preparation of AgNP on 4-aminophenyl modified HOPG surface as described in Ref. [70]

diameter of the AgNP synthesized in this way is about 12 nm, as determined by TEM. The UV-vis absorption spectrum of fresh prepared AgNP showed a sharp absorption band at 410 nm. However, after some hours of aging of the solution, a second absorption maximum at 470 nm was noticed indicating particle aggregation and clustering. These two absorption bands were assigned to the transverse and longitudinal surface plasmon resonance, respectively. These authors also analyzed the fluorescence emission of the sample as a function of the excitation wavelength, and a continuous red-shift of the emission maximum from 540 to 565 nm was observed when the excitation wavelength changes from 380 to 440 nm. Conversely, UV excitation between 230 and 280 nm, yielded emission spectra with maxima fixed about 315 nm. These results suggest that these electrochemically generated AgNP show dual fluorescence emission, where the shorter emission at 315 nm is due to local field enhancement by relaxation of the excited electron and recombination of electrons and holes, while the longer wavelength red shifting bands with the increasing excitation wavelength results from electron interband transitions, see Chap. “[Silver Nanoparticles: From Bulk Material to Colloidal Nanoparticles](#)”.

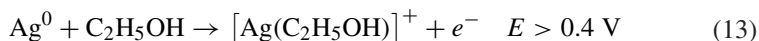
Size and shape control of AgNP has been shown by Ueda et al. and Plieth et al. [72, 80] using a double pulse electroreduction method, which is based on an extremely short nucleation pulse of high cathodic polarization followed by a much longer growth pulse at low cathodic over-voltage (Fig. 15). The ideal model situation is where nucleation only occurs within the first pulse and exclusive particle growth in the second pulse. The high cathodic amplitude of the first pulse is necessary in order to initiate nucleation. Using this method, the conflict between both optimal conditions for nucleation and growth is partially defused. This is due to the amount of small seeds additionally nucleated at the higher polarization and

Fig. 15 Representation of the potentiostatic double-pulse method as described in Ref. [72]

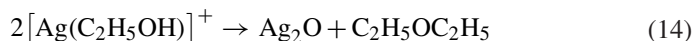


resolved as soon as the potential is switched over to the lower polarization of the growth pulse [72].

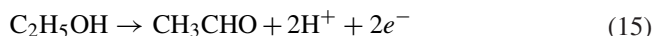
A deposit consisting of AgNP has been obtained by both potentiostatic and galvanostatic methods in non-aqueous solution of NaNO_3 in ethanol ($\text{C}_2\text{H}_5\text{OH}$) as investigated by cyclic voltammetry and chronoamperometry [76]. The proposed mechanism assumes that both anodic dissolution of Ag^0 and its reduction to metallic state proceed during polarization in ethanol according to the following mechanism (Eqs. 13–17) initiated by the Ag^0 one-electron reaction at the surface of the working electrode and solubilization of Ag^+ by $\text{C}_2\text{H}_5\text{OH}$,



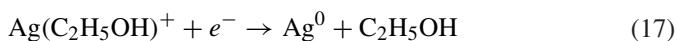
which rapidly decomposes to Ag_2O and ethyl ether (Eq. 14).



The formation and deposition of Ag_2O can partially block the anode. However, at $E > 0.6 \text{ V}$, the oxidation of ethanol occurs forming ethanal (CH_3CHO)



In turn, the aldehyde reduces Ag_2O easily forming Ag atoms (Eq. 16) and the $[\text{Ag}(\text{C}_2\text{H}_5\text{OH})]^+$ is reduced in parallel on the cathode (Eq. 17).



The described process is simple, eco-friendly, requires no expensive instruments, and neither surfactants nor additional reducing agents are needed [76].

Recently, environmentally friendly synthesis of AgNP was also achieved by electroreduction of Ag^+ using PVA as an adequate capping agent [79]. The obtained AgNP were spherical, with a mean diameter of ~ 15 nm as determined by TEM analysis. The use of PVA presents advantages to be considered; low cost, non-toxic, water-soluble, biocompatible and biodegradable. Moreover, the regular linear structure of PVA with a large number of side hydroxyl groups on the main chain suggests excellent hydrophilicity and reactivity. In fact, cyclic voltammetry and FT-IR spectroscopy confirmed that the hydroxyl groups from PVA molecules coordinated with the AgNP, making them more stable during a prolonged period. Thus, AgNP/PVA colloidal dispersions could be utilized for the production of Ag/PVA hydrogels in different forms (thin films, discs and sheets), which could be used for biomedical applications as antimicrobial treatments [79].

Electrochemical methods has been also useful to produce AgNP of different shapes, like nanorods [71], nanoflakes and nanowires [74]. Silver nanorods have been prepared by electroreduction of aqueous solution of AgNO_3 in the presence of polyethylene glycol (PEG) as capping material and further characterized by TEM, X-ray and UV-vis spectroscopy [71]. The results shown that both the concentration of AgNO_3 and PEG can affect the formation of the nanorods.

Nanowires and nanoflakes were prepared by potentiostatic reduction of Ag^+ on HOPG electrode in acetonitrile solution containing mercaptopropionic acid (MPA) [74]. MPA is immediately adsorbed on the deposited silver and affects further growth of the metal. Due to differences in adsorption of thiol molecules onto the various crystallographic facets of silver, some directions of growth are favored and some are inhibited. In consequence, the deposited silver forms rod and flake-like structures which are distributed on the HOPG surface [74].

In summary, most traditional electrochemical methods for production of AgNP have been proven to present some additional advantages over chemical methods in the synthesis of size-selective or shape-controlled highly pure metal nanomaterials, by simple adjusting the current density, solvent conditions, capping agents, etc.

4.1 Sonoelectrochemistry

Combination of ultrasound irradiation and electrochemistry processes date back to the 1930s but in the last decade the expansion of this methodology has become increasingly important. Sonoelectrochemistry is an alternative method, simple and cost effective to obtain AgNP [81]. The diversity of induced effects on electrochemistry processes by ultrasound waves can be attributed to the generation, growth and collapse of microbubbles within the electrolyte [82].

A number of different instrumental setups have been used for the incorporation of the ultrasound irradiation into the electrochemical systems. The first and simplest setup used was the immersion of a conventional electrochemistry cell at a fixed position in an ultrasonic bath. One of the most adequate systems was first described by Reisse et al. [83] (Fig. 16). This system used the simplest configuration of a

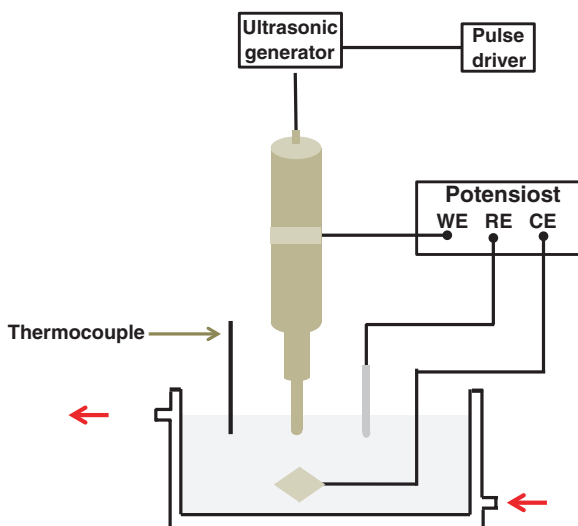


Fig. 16 Sonoelectrochemistry set-up used in the production of nanopowders (*WE* working, *RE* reference and *CE* auxiliary electrode) according to Ref. [81]

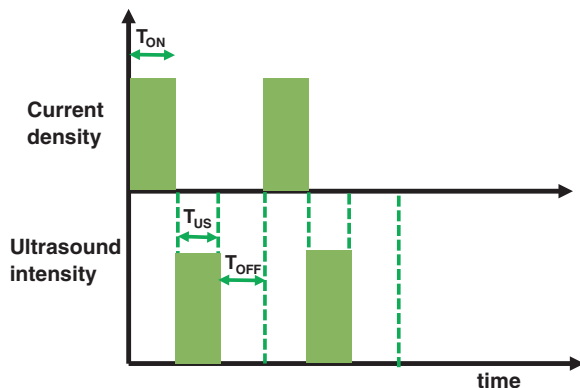
two-electrode cell because the process is under galvanostatic conditions. However, undesirable secondary reactions were observed, and so an adaptation was made. The replacement of the two-electrode configuration (cathode and anode) by a three-electrode configuration (working, reference and auxiliary electrodes) in the sonoelectrochemistry system was performed with the aim of applying a controlled potential to the sonoelectrode to obtain better control over the process.

The fundamental basis of the pulsed sonoelectrochemical technique for the production of nanopowders is massive nucleation. At the cathode, a pulse of current (or potential) reduces a number of cations, depositing a high density of metal nuclei on the sonoelectrode surface, and the titanium horn works only as an electrode during this time (T_{ON}). After this short electrochemical pulse, a short ultrasound pulse of high intensity (T_{US}) removes the metal particles from the cathode surface and replenishes the double layer with metal cations by stirring the solution. Sometimes, a rest time (T_{OFF}) without current or ultrasonic vibrations follows the two previous pulses and it is useful to restore the initial conditions close to the sonoelectrode surface. Figure 17 shows the pulse distribution with time. Electrochemical and ultrasound pulses typically ranges between 100 and 500 ms and the rest time lasts no more than 1 s.

Silver nanoparticles have been synthesized using different electrolytes and stabilizers by the pulsed sonoelectrochemistry method. AgNP with different morphology including spheres, rods and dendrites were prepared from an aqueous solution of $AgNO_3$ in the presence of nitriloacetate (NTA) [84].

Jiang et al. [85] reported the synthesis of silver nanoparticles with a face-centered cubic (fcc) structure in a saturated solution of silver citrate in the presence of PVP.

Fig. 17 Representation of ultrasound and current pulse distribution with time according to Ref. [69]. (T_{ON} current pulse time, T_{US} ultrasound pulse time and T_{OFF} rest time)



Under the experimental conditions used spherical AgNP were prepared with an average diameter of 20–25 nm.

Some of the advantages of this method are: acceleration of mass transport, cleaning and degassing of the electrode surface, and an increased reaction rate [86].

Process yield and particle size are affected by various factors such as the ultrasound pulse time and the current density. In general, decreasing temperature, shorten pulse duration, high current density and high ultrasound intensity will lead to a reduction in crystal size. These parameters need to be optimized in order to maximize the nanoparticles production yield and to obtain the smaller size of the products depending of their applications.

In addition, undesirable side effects like aggregation can be reduced by controlling reactions parameters such as electrodeposition and ultrasound conditions, and by using a suitable stabilizer.

5 Characterization Techniques: What Information Do They Give Us?

Characterizing metallic nanoparticles as AgNP implies determination of their size, shape, chemical composition, and for some applications also their bulk concentration. Next, we summarize the most common techniques used to characterize the synthesized metal nanoparticles including AgNP.

Traditionally, chemical characterization of AgNP has been done using transmission or scanning electron microscopy (TEM/SEM) followed by energy-dispersive X-ray spectroscopy (EDS) and X-ray diffraction (XRD). Also, size exclusion and ion chromatography (SEC and IC) with multi-element detection (inductively-coupled plasma mass spectrometry and optical emission spectroscopy, ICP-MS and ICP-OES, respectively) have been applied because of the intrinsic limitations of Electron Microscopy. Other disadvantages of EM are charging effects (caused

Table 1 Common analytical methods for AgNP characterization

Method	Information	Advantages	Limitations
Turbidimetry/Nephelometry	Concentration with standards	Sample preparation	Low sensitivity (mg/L)
		Non invasive and	
		Non destructive	Sample artifacts
Laser-induced breakdown detection (LIBD)	Concentration size	High sensitivity (µg/L)	Dilute solutions
			Research-grade Instrumentation
			External calibrations
			No elemental information
UV-vis spectroscopy	Concentration	Non invasive	Interferences from turbidity
	Some structural information	Non destructive	
	Elemental composition	Simultaneous elemental composition	Requires acid digestion
Inductively-coupled plasma atomic emission spectroscopy and mass spectrometry ICP-AES/ICP-MS		Very sensitive (µg/L)	Destructive
		Selectivity: MS > AES	Expensive instrumentation
			MS requires expensive instrumentation
Near field scanning optical microscopy (NSOM)	Optical image	Non destructive	Low resolution (diffraction limit of light/size of nanoparticles)
	Size and shape (30 nm level)		
	Size and shape (1–1 µm)	High resolution	Destructive
Scanning electron microscopy (SEM)			Charge effects
			Incompatible with wet or liquid samples
Transmission EM (TEM)/Scanning TEM (STEM)	Size	Very high-resolution	Destructive
	Shape		Charge effects
	Structural information (up to 0.1 nm)		Incompatible with wet or liquid samples
			Expensive instrumentation

(continued)

Table 1 (continued)

Method	Information	Advantages	Limitations
Atomic force microscopy (AFM)	Height	Provides 3D surface plots at sub-nm resolution with adequate instrumentation (type of tip, scanner, excellent signal to noise ratio)	Affected by tip coating and loading Overestimation of lateral dimensions
	Topography (Resolution < 0.1 nm)		
Dynamic light scattering (DLS)	Hydrodynamic diameter (>3 nm)	Simple and rapid analysis	Limited capability for polydisperse samples
Electrophoretic mobility (EM)	Zeta potential (ξ)	Simple and rapid analysis	Interpretation in terms of nanoparticle surface

by accumulation of static electric fields), ~10 % of uncertainties in quantitative analysis and to operate under vacuum conditions [87, 88].

Imaging in fluid solutions is possible using atomic force microscopy (AFM), in which 3D surface profiles can be achieved with height resolutions of ~0.5 nm. The main limitation of AFM is that the geometry of the tip is often larger than the particles being probed and this leads to errors in the onset and offset of particle topography on a scan, resulting in overestimations of the lateral dimensions of the nanoparticles [88].

The spectral response of AgNP in the visible and infrared region of the electromagnetic spectrum has attracted even more attention. The phenomenon known as the surface plasmon resonance (SPR) is localized on the surface of the nanostructure [89]. These resonances stem from the collective oscillation of surface conduction electrons driven by the incident electromagnetic field. The SPR properties of metal nanoparticles are strongly size and shape dependent in addition to capping effects and dielectric constant of the medium, see Chap. “Silver Nanoparticles: From Bulk Material to Colloidal Nanoparticles”. Thus, control over the size and shape of metal nanoparticles is of considerable importance. In a UV-Vis spectrum, the average particle size is associated with the maximum absorption wavelength, while the particle dispersion is related with the full width at half maximum (fwhm) [87].

Scattering techniques like static (SLS) and dynamic light scattering (DLS), or neutron scattering, such as small-angle neutron scattering (SANS) are also useful for nanoparticle characterization. For example, DLS is particularly employed for sizing nanoparticles and determining their state of aggregation in suspensions [90]. Other laser-based techniques include Raman spectroscopy and laser-induced fluorescence (LIF) allowing a better understanding of physical properties [90].

Thermogravimetry and differential thermo analysis (TG-DTA) are useful for investigating the thermal stability and decomposition, dehydration, oxidation, as well as the determination of volatile content and other compositional analysis. TG in combination with a mass spectrometer can be used for surface analysis [90]. Properties of dispersed particles are also studied by electrophoresis in particular, for measuring the zeta potential that informs about the overall charge of a particle and gives an indication of the stability of a colloidal system against agglomeration [90].

In Table 1 are summarized the main methods available for the analysis of AgNP ordered by the information obtained [87, 88, 90].

6 Concluding Remarks

Silver nanoparticles can be obtained by either a top-down or bottom-up approach. Hundreds of research articles reporting different synthetic methods for AgNP are published every year. Throughout this chapter we have reviewed only some of the most relevant works, dealing mostly with bottom-up: chemical reduction, photochemical and electrochemical methods. The particle formation mechanisms were discussed as a key to understand (and predict) the outcome of any synthetic method.

Depending on the AgNP application, the choice of the synthetic route is not a trivial decision as the product (e.g. size and shape) depends on the metal precursor, capping selection, reaction temperature, etc. Nucleation and growth mechanisms do not always follow classical models (La Mer's) as it has been described, for example, in the case of chemical reduction using sodium borohydride, and this affects mainly the final size together with polydispersity. For its part, the polyol method represents a chemical alternative to modulate the shape by selecting the adequate PVP/Ag⁺ concentration ratio.

Light-assisted methods for AgNP are attractive due to their high versatility, selectivity and possibility to have control over the final particles shape and size. Electrochemical methods also permit selection of shape and size by adjusting parameters like current density, solvent conditions, pulse duration, etc.

Finally, we expect this chapter to be helpful on deciding the most appropriate method to synthesize AgNP to accomplish the readers' purposes.

Acknowledgments We want to thank to all the researchers whose work has been cited in here. C.D.B thanks the Agencia de Promoción Científica y Tecnológica (ANPCyT) and Universidad Nacional de Santiago del Estero (UNSE) for combined financial support (PICTO-UNSE-2012-0013). N.L.P and A.V.V would like to thank funding support from CONICET, ANPCyT-PICT 2011-0106, SECYT-UNC and Mincyt-Córdoba. N.P., A.V., V.R., and C.D.B. are research members of the Consejo Nacional de Investigaciones Científicas y Técnicas (CONICET) of Argentina.

References

1. Rogers, K.R., et al.: Alterations in physical state of silver nanoparticles exposed to synthetic human stomach fluid. *Sci. Total Environ.* **420**, 334–339 (2012)
2. Alarcon, E.I., et al.: The biocompatibility and antibacterial properties of collagen-stabilized, photochemically prepared silver nanoparticles. *Biomaterials* **33**(19), 4947–4956 (2012)
3. Lee, P.C., Meisel, D.: Adsorption and surface-enhanced raman of dyes on silver and gold sol. *J. Phys. Chem.* **86**, 3391–3395 (1982)
4. Li, W., et al.: Dimers of silver nanospheres: facile synthesis and their use as hot spots for surface-enhanced raman scattering. *Nano Lett.* **9**, 485–490 (2009)
5. Alvarez-Puebla, R.A., Aroca, R.F.: Synthesis of silver nanoparticles with controllable surface charge and their application to surface-enhanced raman scattering. *Anal. Chem.* **81**, 2280–2285 (2009)
6. Stamplecoskie, K.G., Scaiano, J.: Optimal size of silver nanoparticles for surface-enhanced raman spectroscopy. *J. Phys. Chem. C* **115**, 1403–1409 (2011)
7. Marsich, L., et al.: Poly-L-lysine-coated silver nanoparticles as positively charged substrates for surface-enhanced raman scattering. *Langmuir* **28**, 13166–13171 (2012)
8. Li, J.M., et al.: Detecting trace melamine in solution by SERS using Ag nanoparticle coated poly(styrene-co-acrylic acid) nanospheres as novel active substrates. *Langmuir* **27**(23), 14539–14544 (2011)
9. Wang, B., Zhang, L., Zhou, X.: Synthesis of silver nanocubes as a SERS substrate for the determination of pesticide paraoxon and thiram. *Spectrochim. Acta Part A Mol. Biomol. Spectrosc.* **121**, 63–69 (2014)
10. Hornyak, G.L., et al.: *Introduction to Nanosciences*. CRC Press. Taylor & Francis Group, Boca Raton (2008)

11. Narayanan, K.B., Sakthivel, N.: Biological synthesis of metal nanoparticles by microbes. *Adv. Colloid Interface Sci.* **156**(1–2), 1–13 (2010)
12. Hebbalalu, D., et al.: Greener techniques for the synthesis of silver nanoparticles using plant extracts, enzymes, bacteria, biodegradable polymers, and microwaves. *ACS Sustain. Chem. Eng.* **1**(7), 703–712 (2013)
13. Rycenga, M., et al.: Controlling the synthesis and assembly of silver nanostructures for plasmonic applications. *Chem. Rev.* **111**(6), 3669–3712 (2011)
14. Sun, Y.: Controlled synthesis of colloidal silver nanoparticles in organic solutions: empirical rules for nucleation engineering. *Chem. Soc. Rev.* **42**, 2497–2511 (2013)
15. Sakamoto, M., Fujistuka, M., Majima, T.: Light as a construction tool of metal nanoparticles: synthesis and mechanism. *J. Photochem. Photobiol. C* **10**(1), 33–56 (2009)
16. Cushing, B.L., Kolesnichenko, V.L., Oconnor, C.J.: Recent advances in the liquid-phase syntheses of inorganic nanoparticles. *Chem. Rev.* **104**, 3893–3946 (2004)
17. Vanysek, P.: Electrochemical series. In: Lide, D.R. (ed) *CRC Handbook of Chemistry and Physics*, p. 8.21–8.31. CRC Press, LLC (2003–2004)
18. Hoonacker, A.V., Englebienne, P.: Revisiting silver nanoparticle chemical synthesis and stability by optical spectroscopy. *Curr. Nanosci.* **2**, 359–371 (2006)
19. Hudnall, P.M.: Hydroquinone. In: *Ullmann's Encyclopedia of Industrial Chemistry*. Wiley-VCH Verlag GmbH & Co, KGaA (2000)
20. Turkevich, J., Stevenson, P.C., Hillier, J.: A study of the nucleation and growth processes in the synthesis of colloidal gold. *Discuss. Faraday Soc.* 55–75, (1951)
21. Pillai, Z.S., Kamat, P.V.: What factors control the size and shape of silver nanoparticles in the citrate ion reduction method? *J. Phys. Chem. B* **108**, 945–951 (2004)
22. Henglein, A., Giersig, M.: Formation of colloidal silver nanoparticles: capping action of citrate. *J. Phys. Chem. B* **103**, 9533–9539 (1999)
23. Segur, J.B., Oberstar, H.E.: Viscosity of glycerol and its aqueous solutions. *Ind. Eng. Chem.* **43**(9), 2117–2120 (1951)
24. Steinigeweg, D., Schlücker, S.: Monodispersity and size control in the synthesis of 20–100 nm quasi-spherical silver nanoparticles by citrate and ascorbic acid reduction in glycerol–water mixtures. *Chem. Commun.* **48**(69), 8682–8684 (2012)
25. Caswell, K.K., Bender, C.M., Murphy, C.J.: Seedless, surfactantless wet chemical synthesis of silver nanowires. *Nano Lett.* **3**(5), 667–669 (2003)
26. Van Hyning, D.L., Zukoski, C.F.: Formation mechanisms and aggregation behavior of borohydride reduced silver particles. *Langmuir* **14**, 7034–7040 (1998)
27. Viswanatha, R., Sarma, D.: Growth of nanocrystals in solution. In: Rao, C.N.R., Müller, A. Cheetham A.K. (eds.) *Nanomaterials Chemistry*, p. 139–170. WILEY-VCH, Weinheim (2007)
28. La Mer, V.K., Dinegar, R.H.: Theory, production and mechanism of formation of monodisperse hydrosols. *J. Am. Chem. Soc.* **72**, 4847–4854 (1950)
29. Polte, J., et al.: Formation mechanism of colloidal silver nanoparticles: analogies and differences to the growth of gold nanoparticles. *ACS Nano* **6**(7), 5791–5802 (2012)
30. Wuithschick, M., et al.: Size-controlled synthesis of colloidal silver nanoparticles based on mechanistic understanding. *Chem. Mater.* **25**, 4679–4689 (2013)
31. Perez, M.A., et al.: Hydroquinone synthesis of silver nanoparticles: a simple model reaction to understand the factors that determine their nucleation and growth. *Cryst. Growth Des.* **8**, 1377–1383 (2008)
32. Patakfalvi, R., Dekany, I.: Nucleation and growth of silver nanoparticles monitored by titration microcalorimetry. *J. Therm. Anal. Calorim.* **79**, 587–594 (2005)
33. Yoosaf, K., et al.: In situ synthesis of metal nanoparticles and selective naked-eye detection of lead ions from aqueous media. *J. Phys. Chem. C* **111**, 12839–12847 (2007)
34. Gallardo, O., et al.: Silver oxide particles/silver nanoparticles interconversion: susceptibility of forward/backward reactions to the chemical environment at room temperature. *RSC Adv.* **2**(7), 2923 (2012)

35. Wan, Y., et al.: Quasi-spherical silver nanoparticles: Aqueous synthesis and size control by the seed-mediated Lee-Meisel method. *J. Colloid Interface Sci.* **394**, 263–268 (2013)
36. Wiley, B., Sun, Y., Xia, Y.: Synthesis of silver nanostructures with controlled shapes and properties. *Acc. Chem. Res.* **40**(10), 1067–1076 (2007)
37. Burda, C., et al.: Chemistry and properties of nanocrystals of different shapes. *Chem. Rev.* **105**(4), 1025–1102 (2005)
38. Pastoriza-Santos, I., Liz-Marzán, L.M.: Formation and stabilization of silver nanoparticles through reduction by N,N-Dimethylformamide. *Langmuir* **15**, 948–951 (1999)
39. Pastoriza-Santos, I., Liz-Marzán, L.M.: Synthesis of silver nanoprisms in DMF. *Nano Lett.* **2**(8), 903–905 (2002)
40. Rodríguez-Gattorno, G., et al.: Metallic nanoparticles from spontaneous reduction of silver(I) in DMSO. Interaction between nitric oxide and silver nanoparticles. *J. Phys. Chem. B* **106**, 2482–2487 (2002)
41. Sun, Y., Xia, Y.: Shape-controlled synthesis of gold and silver nanoparticles. *Science* **298**(5601), 2176–2179 (2002)
42. Sun, Y., et al.: Polyol synthesis of uniform silver nanowires: a plausible growth mechanism and the supporting evidence. *Nano Lett.* **3**(7), 955–960 (2003)
43. Sun, Y., et al.: Uniform silver nanowires synthesis by reducing AgNO₃ with ethylene glycol in the presence of seeds and poly(Vinyl Pyrrolidone). *Chem. Mater.* **14**, 4736–4745 (2002)
44. Wiley, B., et al.: Polyol synthesis of silver nanoparticles: use of chloride and oxygen to promote the formation of single-crystal, truncated cubes and tetrahedrons. *Nano Lett.* **4**(9), 1733–1739 (2004)
45. Lin, J.-Y., Hsueh, Y.-L., Huang, J.-J.: The concentration effect of capping agent for synthesis of silver nanowire by using the polyol method. *J. Solid State Chem.* (2014)
46. Tao, A., Habas, S., Yang, P.: Shape control of colloidal metal nanocrystals. *Small* **4**(3), 310–325 (2008)
47. Wiley, B., et al.: Shape-controlled synthesis of metal nanostructures: the case of silver. *Chem. Eur. J.* **11**(2), 454–463 (2005)
48. Stamplecoskie, K., Scaiano, J.: Silver as an example of the applications of photochemistry to the synthesis and uses of nanomaterials. *Photochem. Photobiol.* **88**(4), 762–768 (2012)
49. Mafuné, F., et al.: Structure and stability of silver nanoparticles in aqueous solution produced by laser ablation. *J. Phys. Chem. B* **104**(35), 8333–8337 (2000)
50. Bae, C.H., Nam, S.H., Park, S.M.: Formation of silver nanoparticles by laser ablation of a silver target in NaCl solution. *Appl. Surf. Sci.* **197–198**, 628–634 (2002)
51. Tsuji, T., Okazaki, Y., Tsuji, M.: Photo-induced morphological conversions of silver nanoparticles prepared using laser ablation in water—Enhanced morphological conversions using halogen etching. *J. Photochem. Photobiol. A* **194**(2–3), 247–253 (2008)
52. Jiménez, E., et al.: A novel method of nanocrystal fabrication based on laser ablation in liquid environment. *Superlattices Microstruct.* **43**(5–6), 487–493 (2008)
53. Hada, H., et al.: Photoreduction of silver ion in aqueous and alcoholic solutions. *J. Phys. Chem.* **80**(25), 2728–2731 (1976)
54. Guang-Nian, X., et al.: Preparation and characterization of stable monodisperse silver nanoparticles via photoreduction. *Colloids Surf. A* **320**(1–3), 222–226 (2008)
55. Huang, H.H., et al.: Photochemical formation of silver nanoparticles in poly(N-vinylpyrrolidone). *Langmuir* **12**(4), 909–912 (1996)
56. Gaddy, G.A., et al.: Photogeneration of silver particles in PVA fibers and films. *J. Clust. Sci.* **12**(3), 457–471 (2001)
57. Huang, H.T., Yang, Y.: Preparation of silver nanoparticles in inorganic clay suspensions. *Compos. Sci. Technol.* **68**(14), 2948–2953 (2008)
58. Chegel, V., et al.: Ag nanoparticle-poly(acrylic acid) composite film with dynamic plasmonic properties. *Aust. J. Chem.* **65**(9), 1223–1227 (2012)
59. Scaiano, J.C., et al.: Photochemical routes to silver and gold nanoparticles. *Pure Appl. Chem.* **81**(4), 635–647 (2009)

60. Scaiano, J.C., et al.: Magnetic field control of photoinduced silver nanoparticle formation. *J. Phys. Chem. B* **110**(26), 12856–12859 (2006)
61. Alarcon, E., et al.: Human serum albumin as protecting agent of silver nanoparticles: role of the protein conformation and amine groups in the nanoparticle stabilization. *J. Nanopart. Res.* **15**(1), 1374 (2013)
62. Jockusch, S., et al.: Photochemistry and photophysics of α -Hydroxy ketones. *Macromolecules* **34**(6), 1619–1626 (2001)
63. Gonzalez, C.M., Liu, Y., Scaiano, J.C.: Photochemical strategies for the facile synthesis of gold-silver alloy and core-shell bimetallic nanoparticles. *J. Phys. Chem. C* **113**(27), 11861–11867 (2009)
64. McGilvray, K.L., et al.: Photochemical strategies for the seed-mediated growth of gold and gold—silver nanoparticles. *Langmuir* **28**(46), 16148–16155 (2012)
65. Maretti, L., et al.: Facile photochemical synthesis and characterization of highly fluorescent silver nanoparticles. *J. Am. Chem. Soc.* **131**(39), 13972–13980 (2009)
66. Stamplecoskie, K.G., Scaiano, J.: Kinetics of the formation of silver dimers: early stages in the formation of silver nanoparticles. *J. Am. Chem. Soc.* **133**(11), 3913–3920 (2011)
67. Callegari, A., Tonti, D., Chergui, M.: Photochemically grown silver nanoparticles with wavelength-controlled size and shape. *Nano Lett.* **3**(11), 1565–1568 (2003)
68. Stamplecoskie, K.G., Scaiano, J.: Light emitting diode irradiation can control the morphology and optical properties of silver nanoparticles. *J. Am. Chem. Soc.* **132**(6), 1825–1827 (2010)
69. Rodríguez-Sánchez, L., Blanco, M.C., Lopez-Quintela, M.: Electrochemical synthesis of silver nanoparticles. *J. Phys. Chem. B* **104**(41), 9683–9688 (2000)
70. Tang, Z., et al.: Electrochemical synthesis of Ag nanoparticles on functional carbon surfaces. *J. Electroanal. Chem.* **502**(1–2), 146–151 (2001)
71. Zhu, J.-J., et al.: Preparation of silver nanorods by electrochemical methods. *Mater. Lett.* **49**(2), 91–95 (2001)
72. Ueda, M., et al.: Double-pulse technique as an electrochemical tool for controlling the preparation of metallic nanoparticles. *Electrochim. Acta* **48**(4), 377–386 (2002)
73. Ma, H., et al.: Synthesis of silver and gold nanoparticles by a novel electrochemical method. *Chem. Phys. Chem.* **5**(1), 68–75 (2004)
74. Mazur, M.: Electrochemically prepared silver nanoflakes and nanowires. *Electrochem. Commun.* **6**(4), 400–403 (2004)
75. Jian, Z., Xiang, Z., Yongchang, W.: Electrochemical synthesis and fluorescence spectrum properties of silver nanospheres. *Microelectron. Eng.* **77**(1), 58–62 (2005)
76. Starowicz, M., Stypuła, B., Banaś, J.: Electrochemical synthesis of silver nanoparticles. *Electrochem. Commun.* **8**(2), 227–230 (2006)
77. Hu, M.Z., Easterly, C.E.: A novel thermal electrochemical synthesis method for production of stable colloids of “naked” metal (Ag) nanocrystals. *Mater. Sci. Eng. C* **29**(3), 726–736 (2009)
78. Khaydarov, R., et al.: Electrochemical method for the synthesis of silver nanoparticles. *J. Nanopartic. Res.* **11**(5), 1193–1200 (2009)
79. Surudzic, R., et al.: Electrochemical synthesis of silver nanoparticles in poly(vinyl alcohol) solution. *J. Serb. Chem. Soc.* **78**(12), 2087–2098 (2013)
80. Pliehl, W., et al.: Electrochemical preparation of silver and gold nanoparticles: characterization by confocal and surface enhanced Raman microscopy. *Surf. Sci.* **597**(1–3), 119–126 (2005)
81. Sáez, V., Mason, T.: Sonoelectrochemical synthesis of nanoparticles. *Molecules* **14**(10), 4284–4299 (2009)
82. Compton, R.G., Eklund, J.C., Marken, F.: Sonoelectrochemical processes: a review. *Electroanal* **9**(7), 509–522 (1997)
83. Reisse, J., et al.: Sonoelectrochemistry in aqueous electrolyte: a new type of sonoelectroreactor. *Electrochim. Acta* **39**(1), 37–39 (1994)

84. Zhu, J., et al.: Shape-controlled synthesis of silver nanoparticles by pulse sonoelectrochemical methods. *Langmuir* **16**, 6396–6399 (2000)
85. Jiang, L.-P., et al.: A novel route for the preparation of monodisperse silver nanoparticles via a pulsed sonoelectrochemical technique. *Inorg. Chem. Commun.* **7**(4), 506–509 (2004)
86. Mason, T.J., Lorimer, J.P., Walton, D.J.: Sonoelectrochemistry. *Ultrasonics* **28**(5), 333–337 (1990)
87. Liu, J., et al.: Methods for separation, identification, characterization and quantification of silver nanoparticles. *TrAC Trends Anal. Chem.* **33**, 95–106 (2012)
88. Ferreira da Silva, B., et al.: Analytical chemistry of metallic nanoparticles in natural environments. *TrAC, Trends Anal. Chem.* **30**(3), 528–540 (2011)
89. Zheng, X., et al.: Photochemical formation of silver nanodecahedra: structural selection by the excitation wavelength. *Langmuir* **25**, 3802–3807 (2009)
90. Tiede, K., et al.: Detection and characterization of engineered nanoparticles in food and the environment. *Food Addit. Contam.* **25**, 795–821 (2008)

Silver Nanoparticle Applications
In the Fabrication and Design of Medical and
Biosensing Devices

Alarcon, E.; Griffith, M.; Udekwu, K.I. (Eds.)

2015, XIV, 146 p. 63 illus., 36 illus. in color., Hardcover

ISBN: 978-3-319-11261-9